Check for updates

How to cite: *Angew. Chem. Int. Ed.* **2022,** *61,* e202208591
International Edition: doi.org/10.1002/anie.202208591
German Edition: doi.org/10.1002/ange.202208591

Supramolecular Chemistry

Circularly Polarized Luminescence in a Möbius Helicene Carbon Nanohoop**

*Juraj Malinčík, Sudhakar Gaikwad, Juan P. Mora-Fuentes, Marc-Aurèle Boillat, Alessandro Prescimone, Daniel Häussinger, Araceli G. Campaña, and Tomáš Šolomek**

Abstract: We present the first helicene carbon nanoohop that integrates a [6]helicene into [7]cycloparaphenylene. The [6]helicene endows the helicene carbon nanohoop with chiroptical properties and configurational stability typical for higher helicenes, while the radially conjugated seven *para*-phenylenes largely determine the optoelectronic properties. The structure of the helicene carbon nanoohop was unambiguously characterized by NMR, MS and X-ray analysis that revealed that it possesses a topology of a Möbius strip in the solid state and in solution. The chirality transfers from the [6]helicene to the *para*-phenylenes and leads to a pronounced circular dichroism and bright circularly polarized luminescence, which is affected by the structural topology of the nanohoop.

Helicenes are polyaromatic hydrocarbons (PAHs) that consist of *ortho*-fused benzene rings adopting a helical shape.[1] Their inherent chirality and extended π-conjugation leads to strong electronic circular dichroism (ECD)[2] and circularly polarized luminescence (CPL).[3] Helicenes found applications in asymmetric catalysis, molecular machines, molecular recognition and sensors, polymers or in optoelectronic devices.[4,5] Recently, helicenes have been used for construction of a CP-OLED device.[6] Basic all-carbon helicene emitters, however, suffer from low quantum yields of emission and require substantial synthetic modification, such as introduction of functional groups, extension of the π-conjugated system or doping with heteroatoms, in order to enhance their luminescence properties.[5,7–9]

[*n*]Cycloparaphenylenes ([*n*]CPPs), also known as carbon nanohoops, are known for their unique size-dependent optoelectronic properties, which are a consequence of their curved nature and radial π-electron conjugation.[10–12] Unlike carbohelicenes, they display fluorescence with high quantum yields, spectrum of which shifts bathochromically with decreasing number of *p*-phenylenes. The fluorescence quantum yields also decrease with the size of CPPs and those with $n \leq 7$ are non-fluorescent due to the forbidden nature of the $S_1 \rightarrow S_0$ transition.[11–13] The fluorescence can be restored by replacing a phenylene ring in the structure of CPPs with PAHs lowering the molecular symmetry.[14–16] Examples of chiral carbon nanohoops that can thereby emerge, incorporating acenes,[13,17–21] aromatic heterocycles,[22] and others,[23,24] were investigated both theoretically and experimentally. However, the individual subunits in carbon nanohoops are connected via C–C single bonds and, therefore, have typically low enantiomerization barriers, which hampers the separation and characterization of enantiomers. Strategies to achieve configurationally stable nanohoops by introducing a unit with an axial chirality[25–33] or by topological manipulation forming a molecular knot[34] have appeared recently. As a result, some examples displayed a promising CPL.[20,21,26,27,31–33]

Here, we investigate the first helicene carbon nanohoop **1** (Scheme 1) with [6]helicene integrated into [7]CPP. A combination of the planar and radial π-conjugated units results in a Möbius topology of **1** in the solid state and in solution. Nevertheless, the properties of **1** are largely dictated by its individual subunits. The [6]helicene endows **1** with chiroptical properties and configurational stability typical for higher helicenes, while [7]CPP determines the optoelectronic properties. However, the chirality transfer from the [6]helicene leads to a pronounced circular dichroism and bright CPL. In addition, we provide experimental and theoretical evidence that also the topology in **1** affects the chiroptical response observed in the CPL.

The synthesis of **1** (Scheme 1) follows the strategy for [*n*]CPPs developed by Jasti et al.[35] We started from the commercially available 2,7-dibromonaphthalene, which was transformed to naphthalene-2,7-dicarbaldehyde via Bou-

[*] J. Malinčík, Dr. S. Gaikwad, M.-A. Boillat, Dr. A. Prescimone, Dr. D. Häussinger, Prof. Dr. T. Šolomek
Department of Chemistry, University of Basel
St. Johann's-Ring 19, 4056 Basel (Switzerland)
Prof. Dr. T. Šolomek
Department of Chemistry, Biochemistry and Pharamaceutical Sciences, University of Bern
Freiestrasse 3, 3012 Bern (Switzerland)
E-mail: tomas.solomek@unibe.ch
Dr. J. P. Mora-Fuentes, Prof. Dr. A. G. Campaña
Department of Organic Chemistry, University of Granada
Avda Fuentenueva, s/n, 18071 Granada (Spain)
J. Malinčík, Prof. Dr. T. Šolomek
Prievidza Chemical Society
M. Hodžu 10/16, 971 01 Prievidza (Slovakia)

[**] A previous version of this manuscript has been deposited on a preprint server (https://doi.org/10.26434/chemrxiv.13817498.v1).

© 2022 The Authors. Angewandte Chemie International Edition published by Wiley-VCH GmbH. This is an open access article under the terms of the Creative Commons Attribution Non-Commercial License, which permits use, distribution and reproduction in any medium, provided the original work is properly cited and is not used for commercial purposes.

© 2022 The Authors. Angewandte Chemie International Edition published by Wiley-VCH GmbH

15213773, 2022, 37, Downloaded from https://onlinelibrary.wiley.com/doi/10.1002/anie.202208591 by Universitaetsbibliothek Basel Fachstelle E-Medie, Wiley Online Library on [19/01/2023]. See the Terms and Conditions (https://onlinelibrary.wiley.com/terms-and-conditions) on Wiley Online Library for rules of use; OA articles are governed by the applicable Creative Commons License

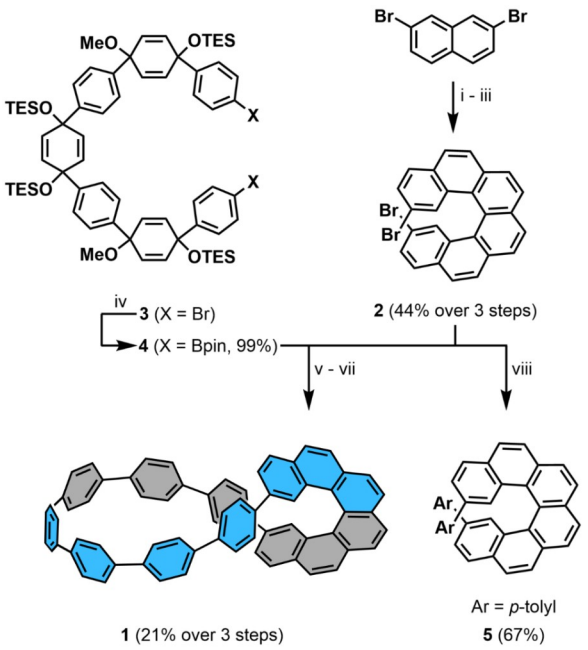

Scheme 1. Synthesis of compounds **1** and **5**: i) a) *n*-BuLi, THF, −78 °C, 1 h. b) DMF, −78 °C to r.t.; ii) (4-bromobenzyl)triphenylphosphonium bromide, NaH, THF, r.t., 16 h; iii) propylene oxide, I_2, toluene, *hν*, r.t., 4.5 h; iv) a) *n*-BuLi, THF, −78 °C, 1 h. b) *i*-PrOBpin, −78 °C to r.t.; v) Pd SPhos G3, K_3PO_4, dioxane/H_2O (10:1), 80 °C, 16 h; vi) TBAF, THF, r.t., 1 h; vii) H_2SnCl_4, THF, r.t., 1 h; viii) *p*-toluneboronic acid, Pd SPhos G3, K_3PO_4, dioxane/H_2O (10:1), 80 °C, 24 h.

veault formylation[36] followed by a double Wittig reaction with (4-bromobenzyl)-triphenylphosphonium bromide and subsequent Mallory cyclization.[37] This sequence afforded 2,15-dibromo[6]helicene **2** in 44 % overall yield over the three steps (Scheme S1). The synthesis of oligo-*p*-phenylene building block commenced from the previously reported compound **3**,[16] which was transformed to diboronate **4** via a double lithium–bromine exchange followed by quenching with *i*-PrOBpin in 99 % yield. The double Suzuki–Miyaura cross-coupling of **2** and **4** followed by deprotection of the silyl protecting groups and subsequent reductive aromatization[38] afforded the target compound **1** in 21 % yield over the three steps. So far, our attempts to isolate the intermediate macrocycle (Scheme S2) before the aromatization step have not been successful and we observed a decomposition of the material during column and gel permeation chromatographies. In order to understand the chiroptical properties of **1**, we synthesized the model [6]helicene **5** by Suzuki–Miyaura cross-coupling of *p*-toluneboronic acid with **2** in 67 % yield.

Compound **1** was characterized by high-resolution mass spectrometry and ^{1}H, ^{13}C, and 2D NMR spectroscopies (see the Supporting Information). Yellow needle-shaped single crystals of racemic **1** were grown by layering a chlorobenzene solution with methanol under argon at room temperature. The single crystal X-ray analysis showed that **1** crystallized in monoclinic $P2_1/n$ space group with unit cell: $a = 18.1064(5)$ Å, $b = 12.6406(2)$ Å, $c = 23.3714(6)$ Å, $\beta = 104.885(2)°$, $\alpha = \gamma = 90°$. It unambiguously confirmed the structure of **1** (Figure 1), which resembles a shape of an asymmetric figure-eight with a disordered molecule of chlorobenzene in the larger loop formed by the *p*-phenylene units.[39]

A closer inspection of the structure in the solid state reveals that **1** possesses a single non-orientable π-surface, i.e., it represents a structure with a Möbius topology, similar to a few previously reported carbon nanohoop derivatives.[40–44] Polycyclic aromatic hydrocarbons with Möbius topology are uncommon but have sparked particular interest because they are predicted to follow the opposite rules of aromaticity known to Hückel systems.[45–51] The synthesis of many Möbius compounds is often rather complicated, while that of **1** uses a straightforward macrocyclization of well-known building blocks. Helicene carbon nanohoops similar to **1** might thus represent worthwhile synthetic targets to study the effect of topology on the aromaticity if the Möbius topology was conserved also in a solution. Therefore, we studied the conformational dynamics of **1** via variable-temperature (VT) ^{1}H NMR spectroscopy and DFT calculations.

Broadening of ^{1}H NMR signals at 7.5 ppm at room temperature (Figure 2) suggests that **1** interconverts between at least two conformers. Therefore, we conducted a conformational search using DFT to identify possible conformations that could be reached by rotation of individual *p*-phenylene units in **1**. We located conformations with the Hückel topology, which are, however, predicted to be > 5 kcal mol^{-1} higher in energy than the conformer with the Möbius topology (Figures 2 and S16, Table S3) that matches the solid-state structure of **1**. The conformers in the two topologies differ in the orientation of the two *p*-phenylene rings (**A**, Table 1) attached directly to the [6]helicene unit. Nevertheless, the energy proximity of the Möbius and the Hückel conformations in **1** suggests that they can interconvert rapidly in a solution on the NMR time scale. In order to confirm these results, we cooled a sample of **1** in THF-d_8 (Figures 2 and S58) and TCE-d_2 (Figure S52) to support our findings from the DFT calculations. The sharp resonance at 6.34 ppm for *ortho*-protons in the pair of *p*-phenylenes **A** adjacent to [6]helicene broadens upon decreasing the temperature and splits into two individual resonances that can be observed at 168 K at 5.38 and 7.29 ppm (Figures S57–S62). We determined the coalescence temperature $T_c = 190$ K and $\Delta G^{\ddagger} = (8.0 \pm 0.12)$ kcal mol^{-1} for their chemical

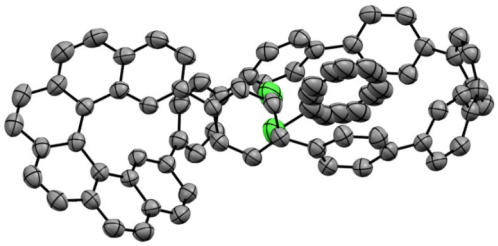

Figure 1. X-ray analysis of *rac*-**1** crystal (*M*-enantiomer is displayed). The thermal ellipsoids are shown at the 50 % probability level.

© 2022 The Authors. Angewandte Chemie International Edition published by Wiley-VCH GmbH

15213773, 2022, 37, Downloaded from https://onlinelibrary.wiley.com/doi/10.1002/anie.202208591 by Universitaetsbibliothek Basel Fachstelle E-Media, Wiley Online Library on [19/01/2023]. See the Terms and Conditions (https://onlinelibrary.wiley.com/terms-and-conditions) on Wiley Online Library for rules of use; OA articles are governed by the applicable Creative Commons License

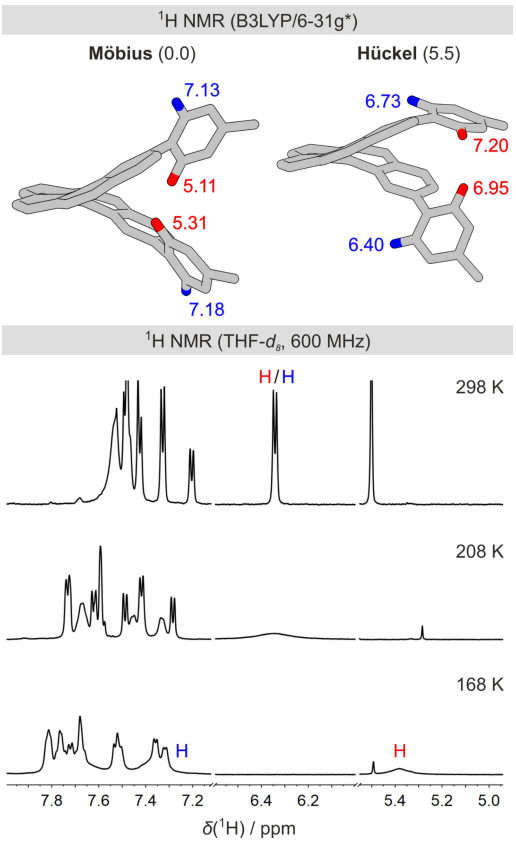

Figure 2. (top) Segment of the structure of the Möbius (left) and Hückel (right) conformations of **1** with the calculated ^{1}H chemical shifts (in ppm) and (bottom) selected spectra from VT ^{1}H NMR experiments of **1** in THF-d_8.

Table 1: Photophysical properties of **1**, **5**, [6]helicene,[52] *m*[8]CPP,[16] and [10]CPP.[12] Strain denotes the strain energy calculated for individual compounds (see text and the Supporting Information). Pairs of individual *p*-phenylene rings in **1** are marked with capital letters. The strain energy stored in individual C–C bonds in **1** increases with the depth of the hue of the red color.

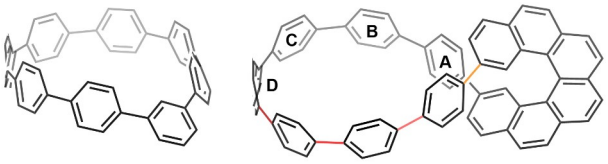

m[8]CPP **1**

Compound	λ_{em} / nm	Φ_{fl}	τ_{fl} / ns	Strain / kcal mol^{-1}
1	490	0.645	4.4	55.4
5	425	0.047	-	–
[6]Helicene	423	0.041	14.5	–
***m*[8]CPP**	484	0.60	3.4	56.7
[10]CPP	466	0.65	6.6	57.7

exchange. These results are in very good accord with the chemical shifts of 5.3 and 7.1 ppm, respectively, obtained from DFT calculations for the Möbius conformer. The NMR rotation barrier also agrees well with the computed value of 5.7–7.8 kcal mol^{-1} (Table S3). In addition, the DFT calculations predict that the chemical shifts for the same proton resonances differ markedly in the Hückel conformers. Our results demonstrate that **1** possesses stable Möbius topology both in the solid state and in a solution with less than 1‰ of **1** in its possible Hückel conformations in the latter. In our case, compound **1**, however, cannot display global Möbius aromaticity because there is an odd number of π electrons in the conjugation path due to the connection of the [6]helicene unit to the *p*-phenylene segment (see Supporting Information). Nevertheless, the stable Möbius topology in related helicene nanohoops makes these compounds attractive to investigate non-linear optical properties as proposed recently by Lu et al. for topologically less stable Möbius phenanthroline carbon nanohoops.[42]

We observed the coalescence also for other proton resonances in **1**. We determined the $T_c = 248$ K and $\Delta G^{\ddagger} = (11.4 \pm 0.12)$ kcal mol^{-1} for the protons at 7.36 and 7.69 ppm (*p*-phenylenes **B**, Table 1), while the rotation of the two remaining *p*-phenylene rings (**C** and **D**) required heating of the NMR sample above room temperature (Figure S52). However, the comparable chemical shifts of the protons in these rings prevented us from determining the exact coalescence temperatures. Nevertheless, we observed that the individual rotational barriers increase with the distance of the *p*-phenylene from the [6]helicene unit (**D** > **C** > **B** > **A**) and correlate with the distribution of the strain energy within the *p*-phenylenes half-loop in **1** (Table 1 and Figure S15). Thus, a higher strain stored in the C–C single bonds connecting the *p*-phenylene rings corresponds to a higher activation free energy of rotation around these bonds. We calculated the strain energy in **1** using StrainViz software,[53] and the homodesmotic reaction depicted in Scheme S3. We obtained the total strain energies (Table 1) of 55.6 kcal mol^{-1} and 55.4 kcal mol^{-1}, respectively, that compare well to those found for *m*[8]CPP (56.7 kcal mol^{-1})[16] or [10]CPPs (57.7 kcal mol^{-1}),[54] although our values neglect part of the strain in the [6]helicene moiety in **1**.

The absorption and emission spectra (Figure 3) of **1** show that its electronic structure differs to that of the [6]helicene **5**. Unlike the vibronically-resolved fluorescence

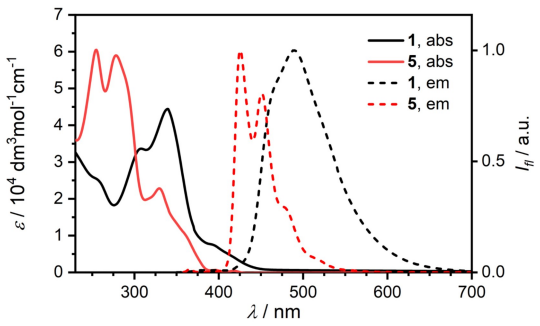

Figure 3. Absorption and emission spectra of **1** (black, $\lambda_{exc} = 339$ nm) and **5** (red, $\lambda_{exc} = 330$ nm) in CH_2Cl_2.

© 2022 The Authors. Angewandte Chemie International Edition published by Wiley-VCH GmbH

15213773, 2022, 37, Downloaded from https://onlinelibrary.wiley.com/doi/10.1002/anie.202208591 by Universitaetsbibliothek Basel Fachstelle E-Media, Wiley Online Library on [19/01/2023]. See the Terms and Conditions (https://onlinelibrary.wiley.com/terms-and-conditions) on Wiley Online Library for rules of use; OA articles are governed by the applicable Creative Commons License

spectrum of **5**, the room temperature emission of **1** is nearly featureless with the emission maximum shifted bathochromically to $\lambda_{em}=490$ nm. The band maximum changes marginally with the polarity of the solvent (Figures S4 and S5). The inspection of the natural transition orbitals (NTOs, Figures S19–S22) of the first two electronic transitions shows that the lowest energy transitions are spatially decoupled but close in energy with a low oscillator strength.

The $S_0 \rightarrow S_1$ is localized in the [6]helicene unit, while the more intense $S_0 \rightarrow S_2$ transition in the curved *p*-phenylene segment. This agrees well with the absorption spectra measured for **1** and **5** ($\approx$400 nm absorption onset, Figure 3). It is expected that the excitation localized in the *p*-phenylene segment will possess a larger reorganization energy when compared to the [6]helicene unit due to a larger release of molecular strain and will likely become the lowest excited state upon geometry relaxation. As a result, the fluorescence characteristic for the CPPs could be observed. Indeed, not only the weak $S_0 \rightarrow S_1$ absorption at $\approx$400 nm and the absorption maximum at 339 nm in **1** match well those in *m*[8]CPP,[11,16] the luminescence spectrum, quantum yield (64.5 %) and the excited state lifetime (4.44 ns, Figures S7 and S8) compare well (Table 1), too. The similarity of the data collected for **1** and *m*[8]CPP[16] can be understood by the comparable curvature (and strain) in these two compounds (Figure S14). Thus, embedding a helicene unit into a CPP augments the emission properties of the helicene.[52]

We then investigated the chiroptical properties that the [6]helicene as a stereogenic element induces in **1**. Because our synthesis uses racemic 2,15-dibromo[6]helicene, we first separated the enantiomers of **1** using HPLC equipped with a chiral stationary phase (Figure S1). The measured ECD spectra of the isolated enantiomers appear as mirror images (Figure 4, top) and we assigned the *M*- and *P*- configurations to the respective enantiomers by TD-DFT calculations (Figures S28–S32). The ECD spectra of the individual enantiomers of **1** and **5** display the Cotton bands with the same signs at comparable wavelengths for the intense electronic transitions (<390 nm). This shows that the chiroptical response in these transitions is dominated by the [6]helicene unit. Comparison of the onset of the ECD spectra, however, reveals that the sign of the weak Cotton band in **1** is opposite to that in **5**. This transition is dominantly localized on the [6]helicene (Figure S19). Indeed, the sign of the transition agrees with the TD-DFT calculations (Table S4) and shows that extending the two phenyls into a closed loop swaps the sign of the Cotton band.

In addition, the chirality transfer from the [6]helicene induces a circularly polarized luminescence (CPL) of the *p*-phenylene segment in the enantiomers of **1** (Figure 4 and S10) that display the CPL of opposite signs. Notably, the signs of the CPL spectra were opposite to the signs of the longest wavelength CD signal, suggesting again a significant geometry reorganization in the excited state. The observed dissymmetry factor $|g_{lum}|=2.2\times10^{-3}$ is comparable to that measured for parent [6]helicene ($\approx1\times10^{-3}$)[6] and other simple helicene derivatives.[3] Figure-of-eight molecules with two helicene units possess g_{lum} values that are an order of magnitude higher but with a commensurate decrease in their luminescence quantum yield.[55,56] Surprisingly, we determined the $|g_{lum}|\approx2\times10^{-2}$ in **5** (Figure S13). Crassous and Favereau et al. reported recently that the presence of electron-donating[6] or electron-withdrawing[57] substituents in the 2,15 positions of [6]helicene results in a similar enhancement of the $|g_{lum}|$ values due to chiral exciton coupling. It is curios that one can achieve a similar effect with two simple tolyl substituents that do not strongly perturb the electronic structure of the [6]helicene and in which a strong exciton coupling is missing. Nevertheless, the combination of the high fluorescence quantum yield and the $|g_{lum}|$ value makes nanohoop **1** a superior CPL emitter in comparison to the simple helicenes and even **5** with a $\approx$10-fold enhanced g_{lum}. This can be demonstrated with the values of CPL brightness B_{CPL},[58,59] which are 63 and 21 for **1** and **5**, respectively.

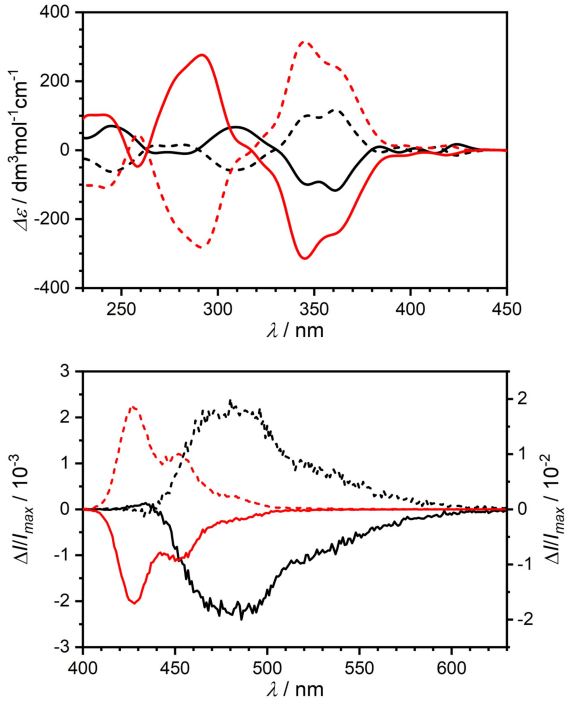

Figure 4. (top) Electronic circular dichroism and (bottom) circularly polarized luminescence spectra of **1** (black, left scale, $\lambda_{exc}=370$ nm) and **5** (red, right scale $\lambda_{exc}=345$ nm) in CH_2Cl_2. (*M*)- and (*P*)-enantiomers are depicted in solid and dashed lines, respectively.

We note that a weak, curious CPL signal with the opposite sign of g_{lum} can be observed at 435 nm. This weak emission suggests that there might be an additional excited state that contributes to the CPL but is not distinguished in the linear fluorescence at room (Figure 3) or low temperature (Figure S9). Excitation spectra (Figure S6) recorded at different emission wavelengths do not show a presence of additional species. The energy of this transition suggests that it could originate from the [6]helicene unit. We optimized the lowest-energy excited states from the Franck–Condon geometry of both the Möbius and Hückel conformers of **1** (Figure S16) using TD-DFT to understand the origin of this

© 2022 The Authors. Angewandte Chemie International Edition published by Wiley-VCH GmbH

15213773, 2022, 37, Downloaded from https://onlinelibrary.wiley.com/doi/10.1002/anie.202208591 by Universitaetsbibliothek Basel Fachstelle E-Medie, Wiley Online Library on [19/01/2023]. See the Terms and Conditions (https://onlinelibrary.wiley.com/terms-and-conditions) on Wiley Online Library for rules of use; OA articles are governed by the applicable Creative Commons License

additional spectral feature in CPL. Geometry relaxation in $\mathbf{1}_{\text{Möbius}}$ fully localizes the excitation in the S_1 state to the *p*-phenylenes (Figure S23), in agreement with our expectation of larger geometry reorganization associated with their curvature in **1**. We do not see any appreciable contribution from the helicene unit in the S_1 state, which confirms a full chirality information transfer from the helicene and reinforces that the luminescence of **1** resembles that in *m*[8]CPP. The calculated sign and value of the g_{lum} also match the experiment (Table S5 and Figure 4). However, the S_1 state NTOs in $\mathbf{1}_{\text{Hückel}}$ show a full localization of the excitation to the [6]helicene (Figure S25). This transition is predicted to be blue-shifted and the sign of the g_{lum} for this putative emission corresponds to the weak signal in the experimental CPL spectrum. Rotation of *p*-phenylenes **A** (Table 1) in the excited state is slow compared to the excited state lifetime. Therefore, the intensity of the signal, missing in the linear fluorescence spectrum, must reflect the Boltzmann distribution of the two topologically different conformers in the ground state at room temperature. The $\approx 5\ \text{kcal mol}^{-1}$ difference at 298 K corresponds to $\approx 5000:1$ ratio of $\mathbf{1}_{\text{Möbius}}$:$\mathbf{1}_{\text{Hückel}}$ in the ground state. Assuming similar absorption coefficients and Φ_{fl}, the value of g_{lum} in $\mathbf{1}_{\text{Hückel}}$ would need to be markedly higher than that in $\mathbf{1}_{\text{Möbius}}$ to be experimentally observable. Indeed, the TD-DFT calculations show $g_{\text{lum}} = -1.23 \times 10^{-2}$, a 5-fold enhancement from that in $\mathbf{1}_{\text{Möbius}}$. Therefore, the ratio of the experimental intensities is expected to be $\approx 1000:1$. Integrating the two bands in the CPL spectrum (Figure 4) yields a ratio of $\approx 100:1$, which is in reasonable agreement considering the assumptions of the model and the initial population ratio estimated by DFT. We thus tentatively attribute the weak signal in the CPL spectrum to the $S_1 \rightarrow S_0$ fluorescence of the topologically distinct $\mathbf{1}_{\text{Hückel}}$. The change in the topology in $\mathbf{1}_{\text{Möbius}}$ lifts the Möbius twist/writhe and necessarily breaks the conjugation between the [6]helicene and the CPP segment, effectively localizing the excitation to the former subunit. As a result, the emission is shifted and the sign of the g_{lum} reverted in comparison to $\mathbf{1}_{\text{Möbius}}$ but also to **5**. It will be interesting to find a system where the two topologically distinct conformations are closer in energy and can interconvert faster to provide additional support to our hypothesis.

Finally, we investigated the configurational stability of **1**. [6]Helicene possesses a high configurational stability[60,61] with a barrier to enantiomerization of $35\ \text{kcal mol}^{-1}$ (DFT: 35–38 kcal mol^{-1}, Table S2). Our calculations predict that the presence of the *p*-phenylene loop increases this barrier in **1** to ≈ 38–$44\ \text{kcal mol}^{-1}$, rendering **1** even more persistent to racemization. This observation is consistent with the concept of persistent chirality of figure-of-eight geometries that involve helicenes.[55,56] Although the chiroptical response of **1** ($\Delta\varepsilon$, Figure 4) is approximately third of that of **5**, our results confirm that the [6]helicene unit endows **1** with similar configurational stability.

In conclusion, we developed a strategy to enhance the luminescence properties of [6]helicene by integrating it into curved [7]cycloparaphenylene, creating a helicene carbon nanohoop **1**. The enantiomers of **1** displayed the chiroptical properties and configurational stability typical for [6]helicene, while the presence of curved *p*-phenylene segment provided the optoelectronic properties comparable to *m*[8]cycloparaphenylene, such as emission of blue-green light with a high quantum yield. We showed, by a combination of X-ray analysis, variable-temperature NMR experiments and DFT calculations that the helicene carbon nanohoop **1** possesses a stable Möbius topology in the solid state and in solution. In addition, the chirality transfer from the [6]helicene induces a bright circularly polarized luminescence in **1**. Finally, we observe that a minor, topologically distinct Hückel conformer of **1** displays a different chiroptical response in CPL. Extension of helicene systems with curved *p*-phenylene segments thus proves to be an efficient strategy to improve the emissive properties of helicenes and chiroptical properties of carbon nanohoops at the same time.

Acknowledgements

We thank Prof. Dr. M. Mayor and the University of Basel for the invaluable support of our research and the SciCore facilities for computational resources. We thank T. Pastierik and Prof. Dr. M. Juríček for their help with the synthesis of [6]helicene and helpful discussions, M. Meyer and B. Pfund for photochemical measurements. This project received funding from the European Research Council (ERC) under the European Union's Horizon 2020 research and innovation programme (Grant Agreements No. 949397 and 677023), the Swiss National Science Foundation (SNSF, PZ00P2_174175, CRSK-2_190341) and the Project PGC2018-101181-B-I00 funded by MCIN/AEI/ 10.13039/ 501100011033 FEDER "Una manera de hacer Europa". Open access funding provided by Universität Bern.

Conflict of Interest

The authors declare no conflict of interest.

Data Availability Statement

The data that support the findings of this study are available in the Supporting Information of this article.

Keywords: Chirality · Circularly Polarized Luminescence · Cycloparaphenylenes · Helicenes · Molecular Nanocarbons · Möbius Topology

[1] R. H. Martin, *Angew. Chem. Int. Ed. Engl.* **1974**, *13*, 649–660; *Angew. Chem.* **1974**, *86*, 727–738.
[2] Y. Nakai, T. Mori, Y. Inoue, *J. Phys. Chem. A* **2012**, *116*, 7372–7385.
[3] W.-L. Zhao, M. Li, H.-Y. Lu, C.-F. Chen, *Chem. Commun.* **2019**, *55*, 13793–13803.
[4] Y. Shen, C.-F. Chen, *Chem. Rev.* **2012**, *112*, 1463–1535.
[5] M. Gingras, *Chem. Soc. Rev.* **2013**, *42*, 1051–1095.

© 2022 The Authors. Angewandte Chemie International Edition published by Wiley-VCH GmbH

15213773, 2022, 37, Downloaded from https://onlinelibrary.wiley.com/doi/10.1002/anie.202208591 by Universitaetsbibliothek Basel Fachstelle E-Medie, Wiley Online Library on [19/01/2023]. See the Terms and Conditions (https://onlinelibrary.wiley.com/terms-and-conditions) on Wiley Online Library for rules of use; OA articles are governed by the applicable Creative Commons License

[6] K. Dhbaibi, L. Abella, S. Meunier-Della-Gatta, T. Roisnel, N. Vanthuyne, B. Jamoussi, G. Pieters, B. Racine, E. Quesnel, J. Autschbach, J. Crassous, L. Favereau, *Chem. Sci.* **2021**, *12*, 5522–5533.
[7] E. Vander Donckt, J. Nasielski, J. R. Greenleaf, J. B. Birks, *Chem. Phys. Lett.* **1968**, *2*, 409–410.
[8] H. Kubo, T. Hirose, K. Matsuda, *Org. Lett.* **2017**, *19*, 1776–1779.
[9] K. Dhbaibi, L. Favereau, J. Crassous, *Chem. Rev.* **2019**, *119*, 8846–8953.
[10] M. Fujitsuka, C. Lu, T. Iwamoto, E. Kayahara, S. Yamago, T. Majima, *J. Phys. Chem. A* **2014**, *118*, 4527–4532.
[11] Y. Segawa, A. Fukazawa, S. Matsuura, H. Omachi, S. Yamaguchi, S. Irle, K. Itami, *Org. Biomol. Chem.* **2012**, *10*, 5979–5984.
[12] E. R. Darzi, R. Jasti, *Chem. Soc. Rev.* **2015**, *44*, 6401–6410.
[13] R. Daengngern, C. Camacho, N. Kungwan, S. Irle, *J. Phys. Chem. A* **2018**, *122*, 7284–7292.
[14] B. M. Wong, J. W. Lee, *J. Phys. Chem. Lett.* **2011**, *2*, 2702–2706.
[15] R. Franklin-Mergarejo, D. O. Alvarez, S. Tretiak, S. Fernandez-Alberti, *Sci. Rep.* **2016**, *6*, 31253.
[16] T. C. Lovell, C. E. Colwell, L. N. Zakharov, R. Jasti, *Chem. Sci.* **2019**, *10*, 3786–3790.
[17] H. Omachi, Y. Segawa, K. Itami, *Org. Lett.* **2011**, *13*, 2480–2483.
[18] J. Wang, G. Zhuang, Q. Huang, Y. Xiao, Y. Zhou, H. Liu, P. Du, *Chem. Commun.* **2019**, *55*, 9456–9459.
[19] P. Della Sala, C. Talotta, M. De Rosa, A. Soriente, S. Geremia, N. Hickey, P. Neri, C. Gaeta, *J. Org. Chem.* **2019**, *84*, 9489–9496.
[20] J. Wang, H. Shi, S. Wang, X. Zhang, P. Fang, Y. Zhou, G.-L. Zhuang, X. Shao, P. Du, *Chem. Eur. J.* **2022**, *28*, e202103828.
[21] J. Wang, G. Zhuang, M. Chen, D. Lu, Z. Li, Q. Huang, H. Jia, S. Cui, X. Shao, S. Yang, P. Du, *Angew. Chem. Int. Ed.* **2020**, *59*, 1619–1626; *Angew. Chem.* **2020**, *132*, 1636–1643.
[22] E. R. Darzi, E. S. Hirst, C. D. Weber, L. N. Zakharov, M. C. Lonergan, R. Jasti, *ACS Cent. Sci.* **2015**, *1*, 335–342.
[23] E. P. Jackson, T. J. Sisto, E. R. Darzi, R. Jasti, *Tetrahedron* **2016**, *72*, 3754–3758.
[24] Y. Wu, G. Zhuang, S. Cui, Y. Zhou, J. Wang, Q. Huang, P. Du, *Chem. Commun.* **2019**, *55*, 14617–14620.
[25] L.-H. Wang, N. Hayase, H. Sugiyama, J. Nogami, H. Uekusa, K. Tanaka, *Angew. Chem. Int. Ed.* **2020**, *59*, 17951–17957; *Angew. Chem.* **2020**, *132*, 18107–18113.
[26] K. Sato, M. Hasegawa, Y. Nojima, N. Hara, T. Nishiuchi, Y. Imai, Y. Mazaki, *Chem. Eur. J.* **2021**, *27*, 1323–1329.
[27] K. Senthilkumar, M. Kondratowicz, T. Lis, P. J. Chmielewski, J. Cybińska, J. L. Zafra, J. Casado, T. Vives, J. Crassous, L. Favereau, M. Stępień, *J. Am. Chem. Soc.* **2019**, *141*, 7421–7427.
[28] T. A. Schaub, E. A. Prantl, J. Kohn, M. Bursch, C. R. Marshall, E. J. Leonhardt, T. C. Lovell, L. N. Zakharov, C. K. Brozek, S. R. Waldvogel, S. Grimme, R. Jasti, *J. Am. Chem. Soc.* **2020**, *142*, 8763–8775.
[29] M. Hermann, D. Wassy, J. Kohn, P. Seitz, M. U. Betschart, S. Grimme, B. Esser, *Angew. Chem. Int. Ed.* **2021**, *60*, 10680–10689; *Angew. Chem.* **2021**, *133*, 10775–10784.
[30] D. Wassy, M. Hermann, J. S. Wössner, L. Frédéric, G. Pieters, B. Esser, *Chem. Sci.* **2021**, *12*, 10150–10158.
[31] M. Krzeszewski, H. Ito, K. Itami, *J. Am. Chem. Soc.* **2022**, *144*, 862–871.
[32] J. He, M. Yu, M. Pang, Y. Fan, Z. Lian, Y. Wang, W. Wang, Y. Liu, H. Jiang, *Chem. Eur. J.* **2022**, *28*, e202103832.
[33] J. Nogami, Y. Nagashima, K. Miyamoto, A. Muranaka, M. Uchiyama, K. Tanaka, *Chem. Sci.* **2021**, *12*, 7858–7865.
[34] Y. Segawa, M. Kuwayama, Y. Hijikata, M. Fushimi, T. Nishihara, J. Pirillo, J. Shirasaki, N. Kubota, K. Itami, *Science* **2019**, *365*, 272–276.
[35] R. Jasti, J. Bhattacharjee, J. B. Neaton, C. R. Bertozzi, *J. Am. Chem. Soc.* **2008**, *130*, 17646–17647.
[36] V. Církva, P. Jakubík, T. Strašák, J. Hrbáč, J. Sýkora, I. Císařová, J. Vacek, J. Žádný, J. Storch, *J. Org. Chem.* **2019**, *84*, 1980–1993.
[37] J. M. Fox, D. Lin, Y. Itagaki, T. Fujita, *J. Org. Chem.* **1998**, *63*, 2031–2038.
[38] V. K. Patel, E. Kayahara, S. Yamago, *Chem. Eur. J.* **2015**, *21*, 5742–5749.
[39] Deposition Number 2178271 contains the supplementary crystallographic data for this paper. These data are provided free of charge by the joint Cambridge Crystallographic Data Centre and Fachinformationszentrum Karlsruhe Access Structures service.
[40] Y.-Y. Fan, D. Chen, Z.-A. Huang, J. Zhu, C.-H. Tung, L.-Z. Wu, H. Cong, *Nat. Commun.* **2018**, *9*, 3037.
[41] S. Nishigaki, Y. Shibata, A. Nakajima, H. Okajima, Y. Masumoto, T. Osawa, A. Muranaka, H. Sugiyama, A. Horikawa, H. Uekusa, H. Koshino, M. Uchiyama, A. Sakamoto, K. Tanaka, *J. Am. Chem. Soc.* **2019**, *141*, 14955–14960.
[42] Z. Liu, T. Lu, *J. Phys. Chem. C* **2020**, *124*, 7353–7360.
[43] K. Li, Z. Xu, J. Xu, T. Weng, X. Chen, S. Sato, J. Wu, Z. Sun, *J. Am. Chem. Soc.* **2021**, *143*, 20419–20430.
[44] Z.-L. Qiu, D. Chen, Z. Deng, K.-S. Chu, Y.-Z. Tan, J. Zhu, *Sci. China Chem.* **2021**, *64*, 1004–1008.
[45] E. Heilbronner, *Tetrahedron Lett.* **1964**, *5*, 1923–1928.
[46] H. S. Rzepa, *Chem. Rev.* **2005**, *105*, 3697–3715.
[47] D. Ajami, O. Oeckler, A. Simon, R. Herges, *Nature* **2003**, *426*, 819–821.
[48] R. Herges, *Chem. Rev.* **2006**, *106*, 4820–4842.
[49] Z. S. Yoon, A. Osuka, D. Kim, *Nat. Chem.* **2009**, *1*, 113–122.
[50] G. Naulet, L. Sturm, A. Robert, P. Dechambenoit, F. Röhricht, R. Herges, H. Bock, F. Durola, *Chem. Sci.* **2018**, *9*, 8930–8936.
[51] X. Jiang, J. D. Laffoon, D. Chen, S. Pérez-Estrada, A. S. Danis, J. Rodríguez-López, M. A. Garcia-Garibay, J. Zhu, J. S. Moore, *J. Am. Chem. Soc.* **2020**, *142*, 6493–6498.
[52] J. B. Birks, D. J. S. Birch, E. Cordemans, E. Vander Donckt, *Chem. Phys. Lett.* **1976**, *43*, 33–36.
[53] C. E. Colwell, T. W. Price, T. Stauch, R. Jasti, *Chem. Sci.* **2020**, *11*, 3923–3930.
[54] Y. Segawa, H. Omachi, K. Itami, *Org. Lett.* **2010**, *12*, 2262–2265.
[55] A. Robert, G. Naulet, H. Bock, N. Vanthuyne, M. Jean, M. Giorgi, Y. Carissan, C. Aroulanda, A. Scalabre, E. Pouget, F. Durola, Y. Coquerel, *Chem. Eur. J.* **2019**, *25*, 14364–14369.
[56] H. Kubo, D. Shimizu, T. Hirose, K. Matsuda, *Org. Lett.* **2020**, *22*, 9276–9281.
[57] K. Dhbaibi, L. Favereau, M. Srebro-Hooper, C. Quinton, N. Vanthuyne, L. Arrico, T. Roisnel, B. Jamoussi, C. Poriel, C. Cabanetos, J. Autschbach, J. Crassous, *Chem. Sci.* **2020**, *11*, 567–576.
[58] L. Arrico, L. Di Bari, F. Zinna, *Chem. Eur. J.* **2021**, *27*, 2920–2934.
[59] Y. Nagata, T. Mori, *Front. Chem.* **2020**, *8*, 448.
[60] R. H. Martin, M.-J. Marchant, *Tetrahedron Lett.* **1972**, *13*, 3707–3708.
[61] J. Barroso, J. L. Cabellos, S. Pan, F. Murillo, X. Zarate, M. A. Fernandez-Herrera, G. Merino, *Chem. Commun.* **2018**, *54*, 188–191.

Manuscript received: June 13, 2022
Accepted manuscript online: July 20, 2022
Version of record online: August 4, 2022

© 2022 The Authors. Angewandte Chemie International Edition published by Wiley-VCH GmbH

15213773, 2022, 37, Downloaded from https://onlinelibrary.wiley.com/doi/10.1002/anie.202208591 by Universitaetsbibliothek Basel Fachstelle E-Medie, Wiley Online Library on [19/01/2023]. See the Terms and Conditions (https://onlinelibrary.wiley.com/terms-and-conditions) on Wiley Online Library for rules of use; OA articles are governed by the applicable Creative Commons License